

# Structural Characterization of the Hot-rolled Ti-25Ta-xZr Alloys by Rietveld Method

Pedro Akira Bazaglia Kuroda<sup>a\*</sup> , Carlos Roberto Grandini<sup>b</sup> , Conrado Ramos Moreira Afonso<sup>a</sup> 

<sup>a</sup>Universidade Federal de São Carlos (UFSCar), Departamento de Engenharia de Materiais (DEMa), 13.565-905, São Carlos, SP, Brasil.

<sup>b</sup>Universidade Estadual Paulista (UNESP), Laboratório de Anelasticidade e Biomateriais, 17.033-360, Bauru, SP, Brasil.

Received: December 15, 2022; Revised: March 31, 2023; Accepted: May 21, 2023

This paper aims to analyze the structure of the Ti-25Ta-xZr system alloys ( $x = 0, 10, 20, 30,$  and  $40\%$  wt.) after melting and hot-rolling by Rietveld's technique. The results confirm that zirconium acts as a  $\beta$  phase stabilizer (in which the Ti-25Ta-40Zr alloy is fully  $\beta$  in the as-cast condition), increases the lattice parameters of the phases, decreases the  $c/a$  ratio of the  $\alpha$  phase, consequently, decreases the elastic modulus values (86 to 72GPa) and decreases the atomic packing factor (APF) of the alloys (60% reduction compared to alloys with and without zirconium in the as-cast condition and 50% reduction in the hot-rolled condition). Concerning hot-rolling, this mechanical process induces the  $\alpha$  phase formation and increases the atomic packing factor of the alloys (APF). By the William-Hall technique, it was possible to calculate the average crystalline size and the micro-strain of the structures.

**Keywords:** *Ti-25Ta-xZr; Rietveld; Structural characterization*

## 1. Introduction

Titanium is a transition metal with an allotropic transformation of around  $883\text{ }^{\circ}\text{C}^{1,2}$ . Below this temperature, its crystalline structure is of the compact hexagonal form (phase  $\alpha$ ). Above this temperature, its structure is the body-centered cubic (phase  $\beta$ )<sup>3-6</sup>. This feature offers the possibility of obtaining alloys with  $\alpha$ ,  $\beta$  or  $\alpha/\beta$  type microstructures, depending on heat treatments and the binding elements that stabilize the phases<sup>7</sup>. Various heat treatments or mechanical conformations are carried out to modify the phases of titanium alloys and improve their mechanical properties for use in the biomedical field, such as hot-rolling<sup>8-10</sup>. The hot-rolling promotes the formation of the martensitic  $\alpha'$  phases. This type of treatment reduces ductility and increases the mechanical and wear resistance of the material<sup>11</sup>.

In titanium alloys, tantalum is considered a  $\beta$ -stabilizing element; it decreases the temperature for the transformation of the  $\beta$  phase<sup>12-15</sup>. Zirconium is considered a neutral element; that is, it does not change the phase transformation temperature of titanium<sup>16-18</sup>. However, recent studies have shown that Zirconium acts as a  $\beta$ -stabilizing element, together with another  $\beta$  element in alloy with titanium<sup>19</sup>.

Kuroda et al.<sup>20</sup> studied the alloys of the Ti-25Ta-Zr system and observed that the crystalline structure of the system is sensitive to the zirconium content; zirconium acts as a  $\beta$  phase stabilizer since its addition in the alloy increases the volumetric fraction of tantalum. However, in their work, a complete characterization of the structure and microstructure was not presented, such as average crystallite size, length of the lattice parameters of each crystalline phase, and percentage of micro-strain. The objective of this

work is to analyze the effect of the substitutional element zirconium and hot rolling on the structure (parameters of the atomic lattice of each phase and packing factor) of alloys of the Ti-25Ta-xZr system ( $x = 0, 10, 20$  and  $30$  and  $40\%$  by weight) by the Rietveld and relate the crystalline structure with the elasticity modulus values and microhardness to understand better the relationships of the phases with the values of mechanical properties.

## 2. Experimental Procedure

The alloys were melted in an arc-melting furnace<sup>21-23</sup>, and then the ingots were submitted to a mechanical hot-rolling process at  $1,273\text{ K}$  with air cooling. The hot-rolling consisted of heating the sample to a temperature of approximately  $1273\text{ K}$ , and then decreasing its initial dimensions and cooling it to air. The sample was finished approximately  $4\text{ mm}$  thick.

X-ray diffraction measurements were performed using a Rigaku, D/Max-2100PC model. The selected method to obtain the diffractograms was the powder method, with Cu-K $\alpha$  radiation ( $\lambda = 1.544\text{ \AA}$ ),  $20\text{ mA}$  current, a potential of  $40\text{ kV}$ , a time of  $1.6\text{ s}$ , and ranging from  $20^{\circ}$  to  $100^{\circ}$ , with a  $0.02^{\circ}$  of step size and fixed time. The structural refinement of Rietveld is a technique that quantifies the diffractograms acquired by the X-ray diffraction technique. From the technique, it is possible to obtain the fraction by weight of individual phases, the lattice parameter, and the distance between the atoms of the alloy<sup>24,25</sup>. For the refinement of the X-ray diffractograms, it was performed using the GSAS program<sup>26</sup>, with EXPEGUI interface<sup>27</sup> and crystallographic data of the  $\alpha$  phase (cod: 43416\_043416) and  $\beta$  (44391\_044391) from the ICDD database. An instrumental file of yttrium oxide ( $\text{Y}_2\text{O}_3$ ) was used to perform the Rietveld analysis.

\*e-mail: [pedro@fc.unesp.br](mailto:pedro@fc.unesp.br)

Williamson-Hall's Equation 1 was used to calculate the size of the crystallite ( $d$ ) and the micro-strain ( $\varepsilon$ ) using Rietveld refinement data.

$$\frac{\beta \cdot \cos \theta}{\lambda} = \frac{1}{D} + \frac{4 \cdot \varepsilon \cdot \sin \theta}{\lambda} \quad (1)$$

where  $\beta$  is the peak width at half the height of the diffraction peak;  $\theta$  is the diffraction angle;  $\lambda$  is the x-ray wavelength;  $D$  is the average size of the crystallite, and  $\varepsilon$  is the micro-strain.

To obtain the images via the optical microscopy (OM) technique, an Olympus optical microscope, the BX51M model, was used. The samples were prepared in advance using a standard metallographic process<sup>28</sup>. The materials were sanded with sandpaper up to 1500 mesh<sup>21</sup>. After mechanically ground, the samples were polished with 1  $\mu\text{m}$  alumina suspension. Kroll's chemical attack solution revealed the sample surfaces (15%  $\text{HNO}_3$ , 5%  $\text{HF}$  and 80%  $\text{H}_2\text{O}$ ).

### 3. Results

The chemical composition results of these materials can be observed in Kuroda et al.<sup>20</sup>. The alloys produced have excellent chemical composition results, with low concentrations of impurities.

Figures 1-5 shows a comparative graph of the X-ray diffraction patterns for as-cast and hot-rolling conditions, together with the images of the simulations performed by the Rietveld technique (a) and micrographs (b).

The X-ray diffractograms were refined by the Rietveld method to quantify the crystalline phases, calculate the lattice parameters, and provide the width to half height ratio of the peaks to calculate the average crystalline size and micro-strain by the Williamson-Hall equation<sup>24</sup>. Figures 1a, 2a, 3a, 4a, and 5a show the refinement results of the diffractograms obtained for each sample. The black line indicates the experimental data of

the diffractograms, the red line indicates the intensity calculated by the refinement, the green line shows the background, and the blue indicates the residue.  $X^2$  is a merit parameter that represents the difference between theoretical data (calculated by Rietveld) compared to experimental data (obtained by x-ray diffraction), where  $X^2$  equals 1 represents an ideal refinement. Data from the literature show that the data obtained in the refinements of this work are adequate<sup>29</sup>.

The visual plot of the refined Ti-25Ta-xZr alloys ensures an excellent fit between the simulated and experimental curves of the samples. Data obtained by the refinements are shown in Table 1.

The results of structural characterization (Figure 1a) showed that after the melting, the alloy with Ti-25Ta presented only peaks of the  $\alpha$  phase, with a hexagonal close-packed (HCP) structure, is a small  $\beta$  peak, with a body-centered cubic structure (BCC) at  $38.16^\circ$  (intensity added to peak  $\alpha$ ). After hot-rolling, peak intensity decreased by  $38.16^\circ$ , indicating a decrease in the  $\beta$  phase count. The micrographs (Figure 1b) as the acicular structural images of the  $\alpha$  phase (basket weave structure). After hot-rolling, there is an increase in the  $\alpha$  phase lamellae and elongated structures in the rolling direction.

The Ti-25Ta-10Zr alloy (Figure 2a) also showed peaks of  $\alpha$  and  $\beta$  phases in both study conditions. In the micrographs (Figure 2b), it is observed that the Ti-25Ta-10Zr alloy is composed of needles that are typical of structures of  $\alpha$  phases and grain characteristic of samples of type  $\beta$ . However, the structures in states of phase needles  $\alpha$  are more refined compared to the micrographs in Figure 1, and the hot-rolling has textured the grain, and there has also been a decrease in grain size.

In Figures 3a, 4a, and 5a, it can be observed that in the Ti-25Ta-20Zr, Ti-25Ta-30Zr, and Ti-25Ta-40Zr alloys. there is the presence of  $\alpha$  and  $\beta$  peaks in the X-ray diffractograms. However, it is noted the decrease in the intensity of the  $\alpha$

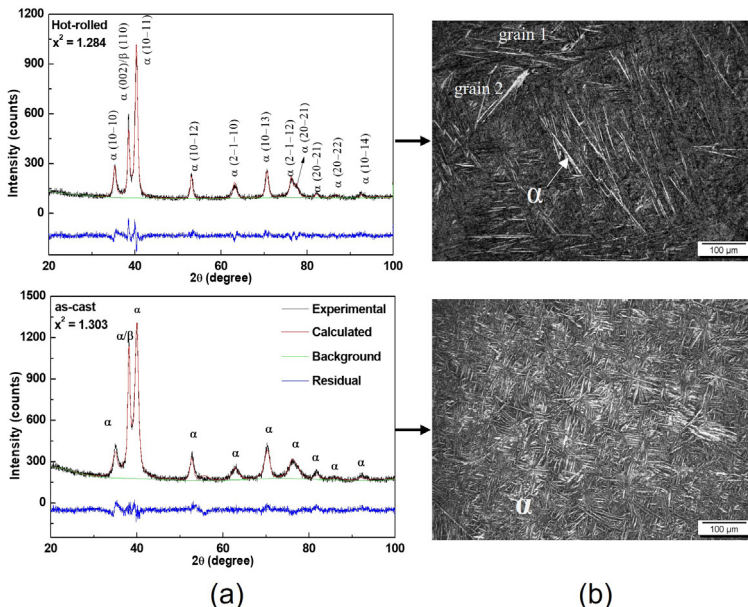


**Figure 1.** XRD patterns refined pattern by Rietveld (a), and micrographs (b) of Ti-25Ta alloy.

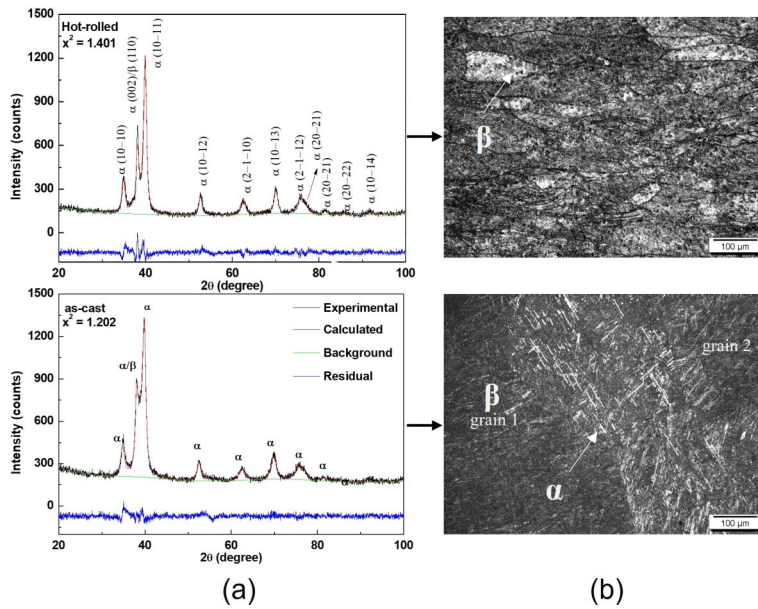


Figure 2. XRD patterns refined pattern by Rietveld (a), and micrographs (b) of Ti-25Ta-10Zr alloy.

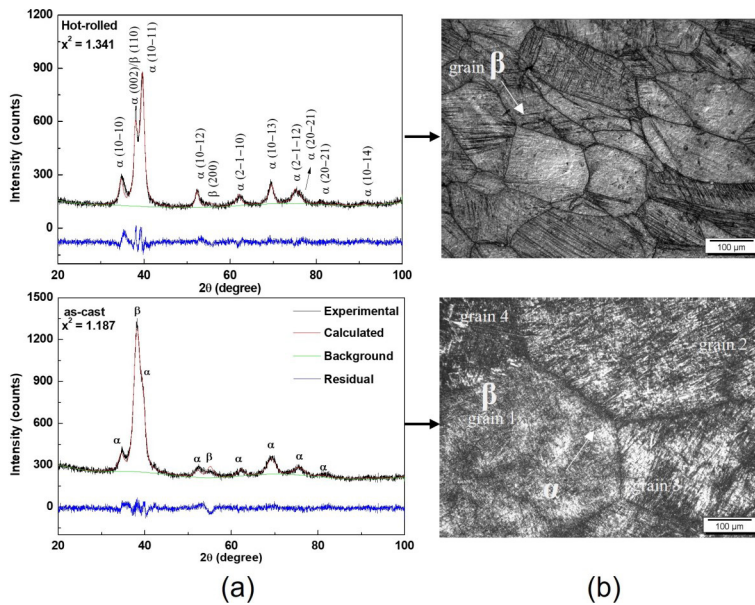


Figure 3. XRD patterns refined pattern by Rietveld (a), and micrographs (b) of Ti-25Ta-20Zr alloy.

phase for the alloys with higher zirconium content, indicating an increase in the percentage of the  $\beta$  phase with the addition of substitutional zirconium in the alloys. It is worth notes, it is noted that the hot-rolling reduces the intensity of the  $\beta$  phase (compared to the results of the as-cast condition), refines and precipitates the formation of the  $\alpha$  phase in  $\beta$ -metastable alloys.

Regarding the micrographs, Figures 3b, 4b, and 5b, it can be observed that the microstructures of the Ti-25Ta-20Zr, Ti-25Ta-30Zr, and Ti-25Ta-40Zr alloys are composed of acicular structures typical of the  $\alpha$  phase and grain  $\beta$  type. It is noting the decrease in  $\alpha$  phase precipitates in alloys with high zirconium content. The micrographs of the alloys

with 20Zr, 30Zr, and 40Zr in the hot-rolling condition did not show  $\alpha$  needles due to the high internal stresses resulting from the mechanical process.

The zirconium acted as a  $\beta$ -stabilizing element, as its increase in high quantities precipitated the formation of the  $\beta$  phase. Therefore, the presence of tantalum ( $\beta$ -stabilizer elements) caused the zirconium to stop acting neutral and start to act in the stabilization of the  $\beta$  phase. Some works have presented similar results confirming the  $\beta$ -stabilizing action of zirconium in Ti-Mo and Ti-Ta alloys<sup>28,30,31</sup>. All images corroborated the experimental results of X-ray diffraction.

Table 1 exhibits the quantitative result of phases by the structural refinement of Rietveld, the lattice parameters of

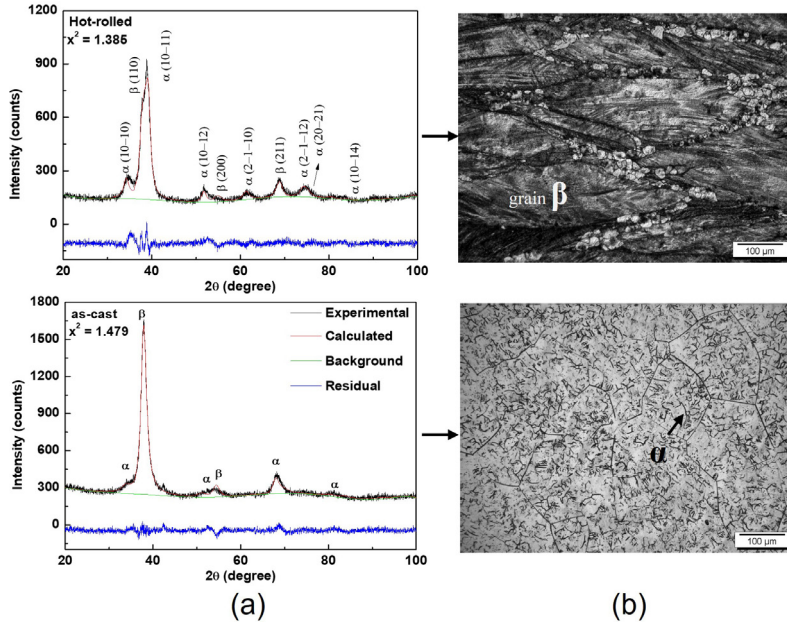


Figure 4. XRD patterns refined pattern by Rietveld (a), and micrographs (b) of Ti-25Ta-30Zr alloy.

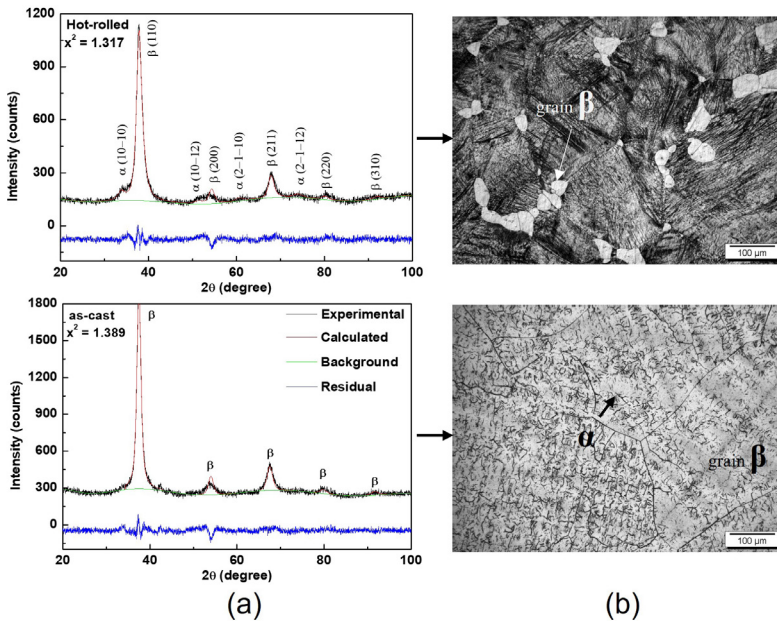


Figure 5. XRD patterns refined pattern by Rietveld (a), and micrographs (b) of Ti-25Ta-40 alloy.

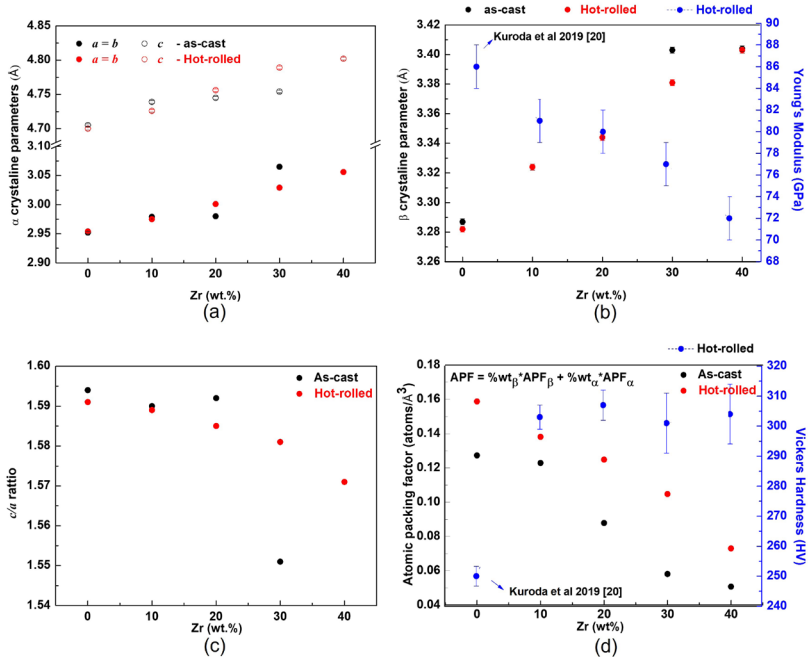
each phase, and the unit cell's volume. Note that adding zirconium in the Ti-25Ta system alloys gradually decreased the percentages of the  $\alpha$  phase and increased the percentage of the  $\beta$  phase, and the hot-rolling induced the formation of the  $\alpha$  phase in the alloys. It is then noted, through Rietveld's structural refinement, that hot rolling promotes the  $\alpha$  phase in the proposed system, unlike other studies in the literature that report that mechanical conformations in titanium alloys induce the formation of the orthorhombic  $\alpha$ '<sup>23</sup>

Regarding the lattice parameters, the zirconium increases the lattice parameter of  $\alpha$  and  $\beta$  phases for both

conditions (Figure 6a, b) due to its greater atomic radius (Zr = 0.159 nm) concerning the other alloy elements (Ti = 0.145 nm and Ta = 0.146 nm), which causes hexagonal close-packed and body-centered cubic structures to be expanded<sup>32-34</sup>. On the other hand, there was a decrease  $c/a$  ratio with the addition of zirconium after hot-rolling (Figure 6c). The values of  $a$ ,  $b$ , and  $c$  change with the hot-rolling because texturing happens. The lattice parameters expand or compress in the preferred rolling direction. Physically the lattice length  $c$  is the variable with the big probability of changes due to its dimension. In this case, the rolling compressed the edge

**Table 1.** Results obtained by Rietveld's refinement.

Sample		Lattice Parameters (Å)				Volume (Å <sup>3</sup> )	phase	%
		<i>a</i>	<i>b</i>	<i>c</i>	<i>c/a</i>			
Ti-25Ta	As-cast	2.952	2.952	4.705	1.594	35.52	$\alpha$	63
		3.287	3.287	3.287	1.000	35.53	$\beta$	37
	Hot-rolled	2.954	2.954	4.700	1.591	35.52	$\alpha$	91
		3.282	3.282	3.282	-	35.35	$\beta$	09
Ti-25Ta-10Zr	As-cast	2.979	2.979	4.739	1.590	36.41	$\alpha$	62
		3.324	3.324	3.324	1.000	36.71	$\beta$	38
	Hot-rolled	2.975	2.975	4.726	1.589	36.22	$\alpha$	75
		3.303	3.303	3.303	1.000	36.05	$\beta$	25
Ti-25Ta-20Zr	As-cast	2.980	2.980	4.745	1.592	36.49	$\alpha$	31
		3.344	3.344	3.344	1.000	37.39	$\beta$	69
	Hot-rolled	3.001	3.001	4.756	1.585	37.09	$\alpha$	66
		3.353	3.353	3.353	1.000	37.69	$\beta$	34
Ti-25Ta-30Zr	As-cast	3.065	3.065	4.754	1.551	38.68	$\alpha$	07
		3.403	3.403	3.403	1.000	39.39	$\beta$	93
	Hot-rolled	3.029	3.029	4.789	1.581	38.05	$\alpha$	50
		3.381	3.381	3.381	-	38.65	$\beta$	50
Ti-25Ta-40Zr	As-cast	-	-	-	-	-	-	-
		3.404	3.404	3.404	1.000	39.45	$\beta$	100
	Hot-rolled	3.056	3.056	4.802	1.571	38.93	$\alpha$	22
		3.403	3.403	3.403	1.000	39.41	$\beta$	77

**Figure 6.** Lattice parameters of phase  $\alpha$  (a),  $\beta$  (b), *c/a* ratio (c), and atomic packing factor (c).

*c* to Ti-25Ta and Ti-25Ta-10Zr alloys and expanded to the other alloys. In other words, rolling in  $\alpha$  titanium alloys decreases the *c* parameter and the unit cell volume. On the other hand, in predominantly  $\beta$  alloys (Ti-25Ta-20Zr, Ti-25Ta-30Zr, and Ti-25Ta-40Zr), the hot-rolling increased the *c* parameter, increasing the unit cell volume. Consequently, there is a decrease in the atomic bonding forces which may indicate that the  $\alpha$ -induced phase by plastic deformations is more sensitive to change.

Due to the increase in the lattice parameters of the crystalline phases, it can be said that zirconium decreases the atomic bond strength; consequently, it decreases the elastic modulus value of the alloys since the modulus value of a material depends on the bond strength between atoms<sup>35</sup>.

As already mentioned, zirconium helps in the stabilization of the  $\beta$  phase and increases the lattice parameters of both phases, so it is assumed that the value of the atomic packing factor (APF) decreases with the zirconium (APF is inversely

proportional to the lattice parameter and zirconium induce the formation of the centered body cubic structure that has a lower APF value compared to the compact hexagonal structure). As the hot-rolling helped the formation of  $\alpha$ , the atomic packing factor grows for this condition (Figure 6d). For this analysis, the authors devised an equation to calculate the atomic packing factor of the titanium alloys according to Equation 2, where  $\%wt_{phase}$  term is the weight percentage of the individual phases, and  $APF_i$  is the packing factor of each

crystalline structure. All terms of the equation can be calculated by the information obtained by the Rietveld technique.

$$APF = \sum_{n=1}^{n_{phases}} (\%wt_{phase.i} * APF_i) \quad (2)$$

Figure 7 illustrates the Williamson-Hall graph of the  $\beta$  phase for all alloys in this study. The crystallite is a set of

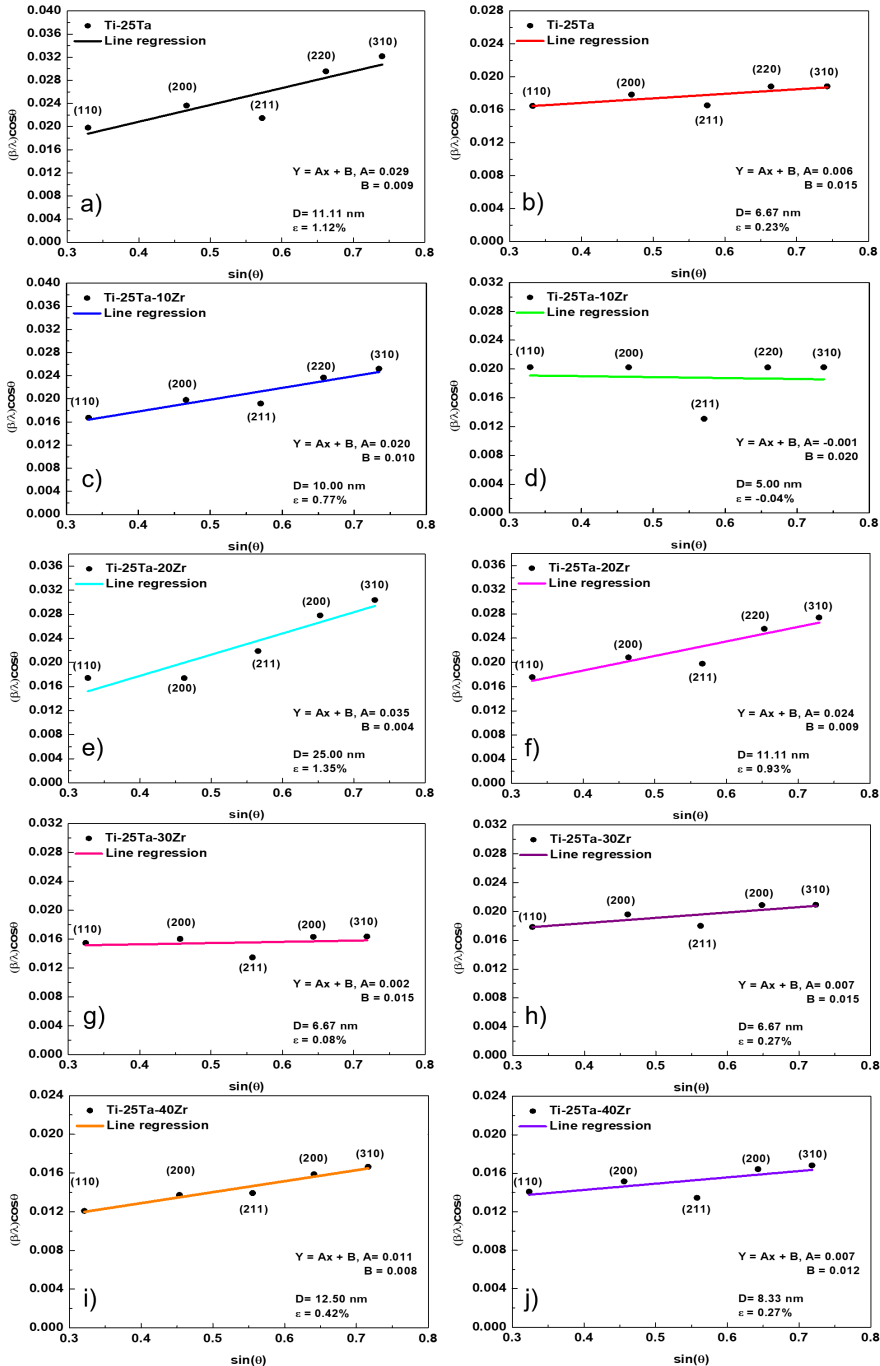


**Figure 7.** Williamson-Hall graph for Ti-25Ta after melting (a) and hot-rolling (b), Ti-25Ta-10Zr after melting (c) and hot-rolling (d), Ti-25Ta-20Zr after melting (e) and hot-rolling (f), Ti-25Ta-30Zr after melting (g) and hot-rolling (h), and Ti-25Ta-40Zr after melting (i) and hot-rolling (j).

cells grouped to form a coherent diffraction domain. Within a metallic grain, several crystallites are grouped in different orientations and sizes, and for all conditions, the crystallites were small ( $D$  between 5 and 25 nm). It is noted that the hot-rolling decreases the average size of the crystallite when metallic material is subjected to mechanical conformation. During the plastic regime, deformation occurs due to the propagation of internal defects, and small breaks in the grains occur. This process can decrease the average size of the crystallite materials. It is worth noting that the unit cell volumes in most alloys also decreased after hot-rolling. This behavior can be observed both in the  $\beta$  and  $\alpha$  phases, corroborating the data obtained of the average crystallite size. Materials with smaller crystalline tend to have smaller unit cell volumes.

Another note is that the micro-strain ( $\epsilon$ ) of  $\beta$  phases decreases. When the materials are subjected to hot-rolling, there is the formation of the  $\alpha$  phase, and as a consequence, there is a decrease in the  $\beta$  phase. In this sense, the appearance of the  $\alpha$  phase in greater quantity contracts the  $\beta$  unit cell, decreasing its micro-deformation value, indicating that the crystalline interface is contracting<sup>24</sup>.

#### 4. Conclusion

From the results presented, it is possible to conclude that:

- The results of X-ray diffraction and microscopy showed that the crystalline structure of the alloys was sensitive to the addition of zirconium and sensitive to hot-rolling.
- Zirconium acted as a  $\beta$  element along with tantalum, and the hot-rolling promoted the  $\alpha$  phase formation.
- Through the Rietveld technique, it was possible to observe that the lattice parameters of the  $\alpha$  and  $\beta$  phases grow with the additional zirconium in the alloy, as a consequence, it increases the elastic modulus of the alloys.
- Zirconium decreased the atomic packing factor of the materials due to the formation of the  $\beta$  phases, which have a lower atomic packing factor than the  $\alpha$  phase, increasing the hardness of the alloys.
- The Williamson-Hall method made it possible to analyze the influence of hot-rolling on the average crystallite size and micro-strain.
- Hot rolling decreases the average crystallite size of the  $\beta$  phase.

#### 5. Acknowledgments

The authors would like to thank the Faculdade de Ciências de Bauru, UNESP, for the XRD and SEM measurements. This study was supported by the following funding agencies FAPESP (São Paulo Research Foundation) grants #2019/26517-6 and through “Projeto Temático” # 2018/18293-8. This study was financed partly by the Coordenação de Aperfeiçoamento de Pessoal de Nível Superior of Brazil (CAPES), Finance Code 001”.

#### 6. References

1. Kaur M, Singh K. Review on titanium and titanium based alloys as biomaterials for orthopaedic applications. *Mater Sci Eng C*. 2019;102:844-62.
2. Sidhu SS, Singh H, Gepreel MA-H. A review on alloy design, biological response, and strengthening of  $\beta$ -titanium alloys as biomaterials. *Mater Sci Eng C*. 2021;121:111661.
3. Geetha M, Singh AK, Asokamani R, Gogia AK. Ti based biomaterials, the ultimate choice for orthopaedic implants – A review. *Prog Mater Sci*. 2009;54(3):397-425.
4. Banerjee D, Williams JC. Perspectives on titanium science and technology. *Acta Mater*. 2013;61(3):844-79.
5. Niinomi M. Mechanical biocompatibilities of titanium alloys for biomedical applications. *J Mech Behav Biomed Mater*. 2008;1(1):30-42.
6. Kuroda PAB, da Silva LM, Sousa KDSJ, Donato TAG, Grandini CR. Preparation, structural, microstructural, mechanical, and cytotoxic characterization of Ti-15Nb alloy for biomedical applications. *Artif Organs*. 2020;44(8):811-7.
7. Lee CM, Ju CP, Chern Lin JH. Structure–property relationship of cast Ti–Nb alloys. *J Oral Rehabil*. 2002;29(4):314-22.
8. Yumak N, Aslantaş K. A review on heat treatment efficiency in metastable  $\beta$  titanium alloys: the role of treatment process and parameters. *J Mater Res Technol*. 2020;9(6):15360-80.
9. Zhu X, Fan Q, Zhou G, Wang D. Influence of hot-rolling on the microstructure and mechanical properties of a near  $\beta$ -type Ti-5.2Mo-4.8Al-2.5Zr-1.7Cr alloy. *Prog Nat Sci*. 2022;32(4):504-9.
10. Jia Z, Zhao Q, Zhang Y, Xu Y, Chen Y, Deng X, et al. Hot and cold rolling of a novel near- $\alpha$  titanium alloy: mechanical properties and underlying deformation mechanism. *Mater Sci Eng A*. 2023;863:144543.
11. Kuroda PAB, Lourenço ML, Correa DRN, Grandini CR. Thermomechanical treatments influence on the phase composition, microstructure, and selected mechanical properties of Ti–20Zr–Mo alloys system for biomedical applications. *J Alloys Compd*. 2020;812:152108.
12. Dercz G. Structure and nanoindentation mechanical properties of novel porous Ti-Ta material with a core-shell structure using the powder metallurgy method. *Adv Powder Technol*. 2019;30(5):1006-17.
13. Zhou YL, Niinomi M, Akahori T. Effects of Ta content on Young’s modulus and tensile properties of binary Ti–Ta alloys for biomedical applications. *Mater Sci Eng A*. 2004;371(1-2):283-90.
14. Zhou Y-L, Niinomi M. Ti–25Ta alloy with the best mechanical compatibility in Ti–Ta alloys for biomedical applications. *Mater Sci Eng C*. 2009;29(3):1061-5.
15. Nicholson WJ. Titanium alloys for dental implants: a review. *Prosthesis*. 2020;2(2):100-16.
16. Correa DRN, Kuroda PAB, Grandini CR. Structure, microstructure, and selected mechanical properties of Ti-Zr-Mo alloys for biomedical applications. *Adv Mat Res*. 2014;922:75-80.
17. Ho WF, Chen WK, Wu SC, Hsu HC. Structure, mechanical properties, and grindability of dental Ti-Zr alloys. *J Mater Sci Mater Med*. 2008;19(10):3179-86.
18. Vicente F, Correa DRN, Donato TAG, Arana-Chavez VE, Buzalaf MAR, Grandini CR. The influence of small quantities of oxygen in the structure, microstructure, hardness, elasticity modulus and cytocompatibility of Ti-Zr Alloys for dental applications. *Materials (Basel)*. 2014;7(1):542-53.
19. dos Santos RF, Rossi MC, Vidilli AL, Amigó Borrás V, Afonso CRM. Assessment of  $\beta$  stabilizers additions on microstructure and properties of as-cast  $\beta$  Ti–Nb based alloys. *J Mater Res Technol*. 2023;22:3511-24.
20. Kuroda PAB, de Freitas Quadros F, Sousa KDSJ, Donato TAG, de Araújo RO, Grandini CR. Preparation, structural, microstructural, mechanical and cytotoxic characterization of as-cast Ti-25Ta-Zr alloys. *J Mater Sci Mater Med*. 2020;31(2):19.
21. Cardoso GC, de Almeida GS, Corrêa DOG, Zambuzzi WF, Buzalaf MAR, Correa DRN, et al. Preparation and characterization

- of novel as-cast Ti-Mo-Nb alloys for biomedical applications. *Sci Rep.* 2022;12(1):11874.
22. Kuroda PAB, Pedroso BLT, Pontes FML, Grandini CR. Effect of titanium addition on the structure, microstructure, and selected mechanical properties of As-Cast Zr-25Ta-xTi alloys. *Metals (Basel).* 2021;11(10):1507.
  23. Cardoso GC, Buzalaf MAR, Correa DRN, Grandini CR. Effect of thermomechanical treatments on microstructure, phase composition, vickers microhardness, and Young's Modulus of Ti-xNb-5Mo alloys for biomedical applications. *Metals (Basel).* 2022;12(5):788.
  24. Severino Martins JR Jr, Grandini CR. Structural characterization of Ti-15Mo alloy used as biomaterial by Rietveld method. *J Appl Phys.* 2012;111(8):083535.
  25. Vicente FB, Correa DRN, Donato TAG, Arana-Chavez VE, Buzalaf MAR, Grandini CR. The Influence of small quantities of oxygen in the structure, microstructure, hardness, elasticity modulus and cytocompatibility of Ti-Zr alloys for dental applications. *Materials (Basel).* 2014;7(1):542-53.
  26. Larson AC, Dreele RBV. General Structure Analysis System (GSAS). New Mexico: Los Alamos National Laboratory; 2004. Report LAUR.
  27. Toby BH. EXPGUI, a graphical user interface for GSAS. *J Appl Cryst.* 2001;34(2):210-3.
  28. Kuroda PAB, Buzalaf MAR, Grandini CR. Effect of molybdenum on structure, microstructure and mechanical properties of biomedical Ti-20Zr-Mo alloys. *Mater Sci Eng C.* 2016;67:511-5.
  29. Banumathy S, Mandal RK, Singh AK. Structure of orthorhombic martensitic phase in binary Ti-Nb alloys. *J Appl Phys.* 2009;106(9):093518.
  30. Correa DRN, Kuroda PAB, Lourenço ML, Grandini CR. Effect of heat treatment in the structure and microstructure of Ti-15Zr-XMo alloys. *Defect Diffus Forum.* 2015;365:305-10.
  31. de Araújo RO, Buzalaf MAR, Grandini CR. Preparation and characterization of Ti-10Mo-xZr alloys for biomedical applications. *Mater Sci Forum.* 2016;869:940-5.
  32. Peters M, Hemptenmacher J, Kumpfert J, Leyens C. Structure and properties of titanium and titanium alloys. In: Leyens C, Peters M, editors. *Titanium and titanium alloys: fundamentals and applications.* Weinheim: Wiley-VCH Verlag GmbH & Co.; 2005. p. 1-36.
  33. Lütjering G, Williams JC. *Titanium.* USA: Springer; 2003.
  34. Lide DR. *Handbook of chemistry and physics.* Boca Raton: CRC Press; 2007.
  35. Shiraishi T, Yubuta K, Shishido T, Shinozaki N. Elastic properties of As-Solidified Ti-Zr binary alloys for biomedical applications. *Mater Trans.* 2016;57(12):1986-92.